Intermetallics 149 (2022) 107680

Contents lists available at ScienceDirect

Intermetallics

journal homepage: www.elsevier.com/locate/intermet

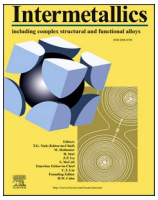

From corrosion behavior to radiation response: A comprehensive biocompatibility assessment of a CoCrMo medium entropy alloy for utility in orthopedic and dental implants

S. Gurel [a], A. Nazarahari [a], D. Canadinc [a,*], G. Gerstein [b], H.J. Maier [b], H. Cabuk [c], T. Bukulmez [d], M. Cananoglu [d], M.B. Yagci [e], S.M. Toker [f,g], S. Gunes [h,i], M.N. Soykan [h,i]

[a] Koc University, Advanced Materials Group (AMG), Department of Mechanical Engineering, Istanbul, 34450, Turkey
[b] Leibniz Universität Hannover, Institut für Werkstoffkunde (Materials Science), An der Universität 2, 30823 Garbsen, Germany
[c] Istinye University, Department of Orthopedics and Traumatology, Istanbul, 34517, Turkey
[d] Istinye University, Department of Radiation Oncology, Istanbul, 34517, Turkey
[e] Koc University Surface Science and Technology Center (KUYTAM), Istanbul, 34450, Turkey
[f] Eskisehir Osmangazi University, Department of Metallurgical and Materials Engineering, Eskisehir, 26480, Turkey
[g] Eskisehir Osmangazi University Translational Medicine Research and Clinical Center, Eskisehir, 26480, Turkey
[h] Eskisehir Osmangazi University Cellular Therapy and Stem Cell Production Application and Research Center (ESTEM), Eskisehir, 26480, Turkey
[i] Eskisehir Osmangazi University, Institute of Health Sciences, Department of Stem Cell, Eskisehir, 26480, Turkey

ARTICLE INFO

Keywords:
CoCrMo
Corrosion
Irradiation
Biocompatibility
Orthopedic implant
Dental implant

ABSTRACT

This paper presents a thorough biocompatibility evaluation of a CoCrMo medium entropy alloy to assess its potential to be utilized in orthopedic and dental implants. For this purpose, a wide range of systematic experiments were carried out, including static immersion, cell culture and radiation experiments. In particular, chemical biocompatibility and ion release behavior of the CoCrMo alloy were studied by carrying out static immersion experiments in artificial saliva (AS), simulated body fluid (SBF) and fetal bovine serum (FBS). Detailed analysis of the surfaces of the tested samples demonstrated that both passive oxide layer and hydroxyapatite formation occur on the CoCrMo sample surfaces immersed in AS, SBF and FBS for 28 days. The response of living cells to the CoCrMo alloy was tested utilizing cell culture experiments, and the evidence of Saos-2 cell viability and proliferation supported the static biocompatibility experiment results, indicating the potential of the CoCrMo alloy to be utilized as an orthopedic implant material. Finally, the effect of a CoCrMo implant on the actual radiation dose induced upon malignant tissue in the vicinity of the implant during a radiotherapy was evaluated by applying medical grade radiation to water phantoms circumventing CoCrMo samples. The results showed that the radiation accumulation in the tissue within the immediate vicinity of a CoCrMo implant would be a minimum, eliminating some of the undesired side effects. Overall, the results of the three different types of experiments reported in this paper have clearly demonstrated that the CoCrMo medium entropy alloy investigated in this study has significant potential to be utilized as a safe implant material in dental and orthopedic implants.

1. Introduction

One of the most common materials used in orthopedic implants is the CoCr alloy owing to its high strength and wear resistance, and long-term durability, which make it the material of choice especially for younger patients undergoing arthroplasty [1]. Specifically, the use of CoCr alloys in arthroplasty has two major purposes: first, they are used as the bearing surface at the articulating part, which could bear a metal-on-metal (MoM) or metal-on-polyethylene (MoP) contact. Secondly, they are employed in the stems or base plates of the implants, where the load is transmitted to the bone. Although at the bearing surface the wear resistance is important, at the stems osteointegration and biomedical fixation are of more importance. For instance, many of the MoM hip implants implanted in significant numbers in the United

* Corresponding author.
E-mail address: dcanadinc@ku.edu.tr (D. Canadinc).

https://doi.org/10.1016/j.intermet.2022.107680
Received 17 January 2022; Received in revised form 19 July 2022; Accepted 1 August 2022
Available online 8 August 2022

Kingdom in the 1960s were mostly replaced with the MoP implants in the mid-1970s as a result of early reports of seizing and loosening. The seizing and loosening of MoM arthroplasties were associated with metal staining due to wear and corrosion of the MoM articulating bearing surfaces [2], and wear debris and metal ions have been associated with this loosening [3]. In particular, these released products may elicit an adverse biological reaction in the host [4], where high ion levels can lead to delayed-type hypersensitivity around the prosthesis to increase lymphocytic infiltration, organ toxicity and carcinogenesis, as well as dermatitis, urticaria and vasculitis [5,6]. In severe cases, increased lymphocytes can even cause bone necrosis and implant failure.

All these problems are mainly facilitated by the release of Cr ions into the bloodstream, which are highly water-soluble and easily permeates the cell membrane through the physiological anion transport channels. Even though Cr ions do not react with DNA in vitro in isolated nuclei, they cause many DNA lesions which include DNA-DNA cross links, DNA-protein cross links and oxidative damage once inside the cell via generating reactive oxygen species [7]. Furthermore, Cr ions have been associated with sarcoma at the implantation site of an orthopedic prosthesis, increased melanoma following implantation of a prosthesis, and increased risk of bladder and ureter cancers [8].

An alternative material to the CoCr alloy is the CoCrMo medium entropy alloy (MEA), especially in the case of arthroplasty [9], and its relatively high strength, modest elastic modulus, and high corrosion and wear resistance have recently made it also popular in the making of dental and orthopedic implants such as screws and pins [10–12]. Even though CoCrMo alloys also contain a significant amount of Cr, which can lead to cytotoxicity if it is released into the human body due to corrosion [13], the CoCrMo alloy also exhibits a natural means of prevention of ion release, such that the Co, Cr and Mo oxides spontaneously form a passive layer on the CoCrMo surface upon contact with the bodily fluids [14,15].

Passive oxide layers form on implant surfaces since they are more stable than the metallic elements themselves, resulting in a barrier between the implant surface and the surrounding environment, which effectively suppresses dissolving of the metallic elements [16–18]. Yet, several factors such as the actual chemical composition of the alloy, the thickness of the passive oxide layer and the mechanical stresses on the surface of the implant affect the corrosion protection performance of the passive oxide layer [11,19]. Moreover, the pH of the surrounding corrosive media can play a significant role, such that low pH values increase the corrosion rate as well as passivation layer solubility [20–24]. Therefore, it is crucial to understand the effect of different corrosive media representing various human body locations to properly assess the usability of potential implant materials.

The corresponding scientific literature offers examples of studies carried out on CoCrMo MEA with this motivation, where ion release and corrosion behaviors of the CoCrMo alloy in solutions imitating human body conditions, including simulated body fluid (SBF). These studies confirm the significant role of solution pH on the corrosion response of the alloy, which can vary based on medical conditions such as inflammation or healing [14,22,24]. An interesting yet important observation was that, regardless of the atomic percentages of the constituent elements, the CoCrMo MEA has a tendency to release Co ions at a significantly higher rate owing to the selective dissolution of Co [25,26]. Specifically, even though the passive oxide layer forming on the CoCrMo MEA primarily consists of Cr oxides, the so called ***Cr-like passivation*** limits the Cr ion release into SBF to a negligible amount [14,26], rather facilitating Co and Mo ion release during corrosion [14,24,25]. A solution-dissolution cycle of the passive oxide layer forming on CoCrMo MEAs was also reported, significantly affecting the rate of ion release from the alloy in the long term [27,28], which can be associated with medical causes such as infection, surgery, the healing process, and other metabolic activities [22,23]. Especially in the case of the oral cavity, the pH can significantly change due to dental plaque formation, and acidic or alkaline nutrition intake, and can significantly decrease towards the 2–3 range when a pathological condition is prevalent [19,23,28–30]. Studies employing artificial saliva (AS) of varying pH to simulate the effects of different oral cavity conditions on the CoCrMo dental implants have demonstrated that a pH value less than 4 significantly enhances ion release from this material in AS [19].

In general, highly corrosive ions inside a corrosive media, such as chloride, determine the thickness and properties of a passive oxide layer forming on an alloy [31]; however, animal studies on CoCrMo MEA [32] have demonstrated that the contribution of proteins to the deterioration of the implant surfaces should also be taken into account when making an assessment of the biocompatibility and corrosion performance of an implant material. For instance, when albumin was added as the protein to the phosphate buffer solution (PBS), Mo release from the CoCrMo MEA increased notably [11]. When the albumin was replaced with alpha calf serum, the corresponding corrosion rates of the CoCrMo MEA in the PBS solution decreased towards clinically more relevant values [33].

A good alternative to PBS solution supplemented by proteins is the fetal bovine serum (FBS), which is a generic serum used as a supplement in biological studies that need to consider the effect of a wide variety of proteins to simulate living body condition when conducting cell growth experiments, a condition that is plausible while healing following an implantation surgery [34–36]. Overall, studies assessing the corrosion response of a variety of implant materials, including a NiTi shape memory alloy [37] and the CoCrMo MEA [38], have clearly shown that the FBS solution enhances the rate of ion release in static biocompatibility experiments owing to the variety of proteins it contains, and thus, constitutes a better environment for characterizing the biocompatibility of metallic implant materials prior to clinical trials.

In the light of the background provided herein, the authors carried out static biocompatibility experiments on the CoCrMo MEA in three different media, namely AS, SBF and FBS, for the sake of a comprehensive bio-corrosion analysis of the CoCrMo MEA and to investigate the passive oxide formation on this potential dental and orthopedic implant material in detail. A thorough set of static biocompatibility experiments, as well as detailed pre- and post-mortem chemical analyses of both the CoCrMo samples and the immersion fluids, were carried out. In addition, to thoroughly assess the biocompatibility of this alloy, cell culture experiments were conducted where Saos-2 cells were cultured on the CoCrMo surfaces in a controlled environment. Finally, considering the long-term utility of the target applications, the reaction of the CoCrMo alloy to different degrees of medical grade radiation was also studied. Overall, the experimental findings presented herein showed that both passive oxide layer and hydroxyapatite formation take place on the CoCrMo MEA upon immersion in AS, SBF and FBS, improving the osseointegration process. While the three different solutions have different effects on the CoCrMo MEA, the CoCrMo MEA demonstrated excellent corrosion resistance against these biological media. Furthermore, cell viability and proliferation on the CoCrMo surface encourage its utility as an orthopedic or dental implant material, which is also supported by the results of the radiation study. The results not only constitute a very comprehensive evaluation of the biocompatibility of the CoCrMo MEA, but also warrant clinical research to approve its utility as implant material in procedures such as total knee arthroplasty or dental implantation.

2. Materials and methods

The CoCrMo MEA (27 wt% Cr, 6 wt% Mo and balance Co) employed in this study was produced by vacuum arc re-melting technique using powders of each element with 99.9% purity. First, button-shaped bulk materials with a diameter of about 60 mm were obtained upon remelting 5 times in a Ti-gettered argon atmosphere on a water-cooled copper crucible. Then, the as-cast bulk alloys were cut by electrical discharge machining (EDM) to obtain discs with a 50.1 mm diameter and a thickness of 6.1 mm. The as-cast CoCrMo alloy discs were then further machined by EDM to obtain 10 mm × 5 mm x 1 mm samples for static

biocompatibility experiments. The surfaces of the EDM-processed samples were mechanically ground using SiC emery papers with grain sizes ranging from 106 to 2.5 μm to eliminate any contamination on the surface, and only a negligible change in the thickness was observed upon mechanical polishing. Subsequently, the samples were polished with 0.3 μm alumina slurry until the surfaces reached a mirror-like appearance, and then the samples were cleaned in an ultrasonic water bath with ethanol and rinsed with de-ionized water. Following preparation, the samples were statically immersed into SBF (pH = 7.4) and AS (pH = 2.3) with the elemental compositions shown in Table 1, and FBS (Biosera FB-1101) for 1, 7, 14 and 28 days [39]. In this process, the CoCrMo MEA samples were placed in sealed tubes which were filled with SBF and AS with a volume-to-surface area ratio of 20 mL/cm^2, and FBS with a volume-to-surface ratio of 10 mL/cm^2. All solutions were kept at a constant temperature of 37 °C throughout the immersion experiments in an electronically controlled water bath to simulate the body temperature.

Following the immersion experiments, the initial microstructural characterization of the CoCrMo MEA samples was conducted by X-ray diffraction (XRD) on a Bruker D2 Advanced X-ray diffractometer. The incidence angle was kept at 5° with a Cu-Kα radiation source which was operated at 30 kV and 10 mA, while the acquisition angle changed from 5° to 90° with a 0.02° increment. To investigate the surface morphology, the samples were analyzed by a Zeiss Ultra Plus field emission scanning electron microscope (SEM) prior to and following the immersion tests. In order to reveal the surface chemistry of the tested samples and inspect the elemental distribution on the sample surfaces following the immersion tests, X-ray photoelectron spectroscopy (XPS) analysis was carried out on the tested samples. The XPS measurements were performed by utilizing a Thermo Scientific K-Alpha spectrometer with an aluminum anode (Al Kα = 1468.3 eV), and the take-off angle was 90° between the sample surface and the axis of the analyzer lens. A flood gun was used to avoid charging. The depth profiling was performed using Ar ion bombardment. Avantage 5.9 software was utilized to perform fitting of the data. The elemental compositions of the immersion solutions following the static immersion experiments were examined by an Agilent 7700x inductively coupled plasma mass spectrometer (ICP-MS) to observe ion release from the immersed samples following 1, 7, 14 and 28 days of immersion.

To assess the interaction of the CoCrMo alloy with living tissue, cell culture experiments were carried out. Saos-2 (ATCC® HTB-85™) cells were bought from the American Type Culture Collection (ATCC, Washington DC, USA). The cells were cultured in Dulbecco's Modified Eagle's Medium (DMEM; Capricorn Scientific, Ebsdorfergrund, Germany), containing heat-inactivated 10% FBS (Capricorn Scientific, Ebsdorfergrund, Germany) and 1% penicillin/streptomycin (Capricorn Scientific, Ebsdorfergrund, Germany) and 1% Glutamax (Gibco™, Massachusetts, USA). The cells were incubated at condition 37 °C in a humidified atmosphere containing 5% CO_2 and 5% O_2. The complete medium was changed once every 3 days over an 8–9-day period. For each passage, the cells were plated similarly and grown to a confluency of 70%. MTT (3-[4,5-dimethylthiazol-2-yl]-2,5 diphenyl tetrazolium bromide) analysis was used to determine cell viability by the presence of mitochondrial activity in the cells. Therefore, 3×10^5 cells were seeded on the metal surfaces of the CoCrMo alloy samples and incubated on these surfaces for 3, 5 and 10 days. At the end of the incubation, the cells were removed from metal surfaces with trypsin-EDTA and inoculated into 96-well plates. MTT solution (Acros Organics B.V.B.A., Massachusetts, USA) at a concentration of 5 mg/ml was added to each well. The cells were then incubated for 3 h in air with 5% CO_2 and 95% relative humidity at 37 °C. After incubation, absorbance values were determined at 540 nm in a microplate reader with a monochromator system (BIOTEK ELx808IU, Vermont, USA). After incubation, the medium was removed and fixed with 2.5% glutaraldehyde (G7651 Sigma-Aldrich, Missouri, USA) for 2 h. It was then dehydrated using ethanol series (50%, 75%, 90% and 96%) and dried under laminar flow. The morphological features of Saso-2 cells on the surfaces of the CoCrMo samples were analyzed using a JEOL JSM-5600LV SEM.

For the irradiation part of the study, the CoCrMo samples were placed on solid water phantoms that simulate live tissue in terms of density and response to radiation. After taking the computer tomography (CT) scans of the samples, the results were incorporated into a Monaco treatment planning system (TPS) for irradiation with 100 cGy utilizing a photon bundle of 6 MV. Point dose radiation measurements were made for lateral distances up to 2 cm from the center of the CoCrMo samples in each direction with an interval of 0.5 cm, and the radiation dose variation from sample surfaces to 2 cm depth from the samples was monitored with a 0.5 cm interval. These treatment plans were verified with the experiments conducted utilizing an IBA Dose 1 electrometer and an IBA FC65 ion capsule on an Elekta Versa HD linear accelerator.

The immersion experiments and the corresponding ICP-MS analyses, as well as the cell culture and radiation experiments were repeated 3 times for each case, where standard deviation remained within 1% for all cases. As for the remaining characterization methods, such as SEM, XRD and XPS, selected samples were studied.

Table 1
Compositions of the AS and SBF utilized in the static immersion experiments.

Solution	Ingredients	Amount (g/L)	pH
AS	NaCl	0.4	2.3
	KCl	0.4	
	$CaCl_2$. $2H_2o$	0.906	
	$NaH_2PO_4.2H_2O$	0.69	
	$Na_2S.9H_2O$	0.005	
	Urea	1	
SBF	NaCl	8.036	7.4
	$NaHCO_3$	0.352	
	KCl	0.225	
	$K_2HPO_4.3H_2O$	0.23	
	$MgCl_2.6H_2O$	0.311	
	1 M HCl	40 mL	
	$CaCl_2$. $2H_2o$	0.293	
	Na_2SO_4	0.072	
	TRIS	6.063	
	1 M HCl	0.2 ml	

3. Results and discussion

3.1. Static biocompatibility and the chemical characterization

The XRD pattern acquired from the as-cast CoCrMo sample is illustrated in Fig. 1. Experimental lattice parameters and peak values of CoCrMo calculated using Bragg's Law revealed that the as-cast CoCrMo alloy contained hexagonal close packed (HCP) and face-centered cubic (FCC) phases, which aligns well with the corresponding literature [40].

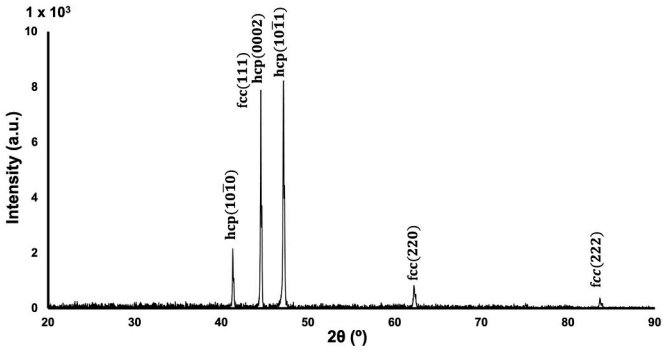

Fig. 1. The XRD pattern showing the coexistence of HCP and FCC phases in the as-cast CoCrMo alloy.

The ICP-MS analysis revealed that Cr release from the CoCrMo alloy is promoted by increased acidity, such that the Cr ion release into the AS solution, which has the lowest pH value of 2.3 among all solutions, was significantly higher as compared to the Cr ion release into SBF and FBS (Fig. 2(a)). Indeed, the Cr ion release into AS was already noteworthy starting with day 1 and continued to increase with time, while a notable ion release into FBS started only following 14 days of immersion and a very stable and low amount of Cr ion release into SBF was detected. When examined closely, the Cr ion concentration released into FBS is observed to have decreased from day 7 to day 14 prior to its notable increase afterwards. This is attributed to the passive oxide layer formation during the second week of immersion, such that the free Cr ions in FBS released during the first week were absorbed into this passive oxide layer while it was forming, which has been previously reported for NiTi shape memory alloys [41]. Nevertheless, the passive oxide layer could not prevent Cr ion release into FBS following the second week, which is attributed to the active proteins in the FBS solution reacting with it.

The Mo ion release into the three immersion solutions is presented in Fig. 2(b). Accordingly, a similar trend of Mo ion release into AS and SBF was observed, yet the quantity of ion release into AS was larger. Furthermore, the rate of ion release into AS and SBF slowed down significantly following the first week of immersion, which is indicative of a passive oxide layer formation. Unlike the AS and SBF, the amount of Mo ions detected in the FBS solution decreased from day 1 to the middle of the second week prior to increasing at a high rate to finally surpass the amount Mo ion release into the more acidic AS solution. This is associated with the fact that Mo ions initially form compounds on the surface of the sample which causes the Mo concentration in the immersion fluid to decrease. However, later on, the ion release surges since the proteins in the FBS react with these compounds, changing the dissolution and passivation mechanisms.

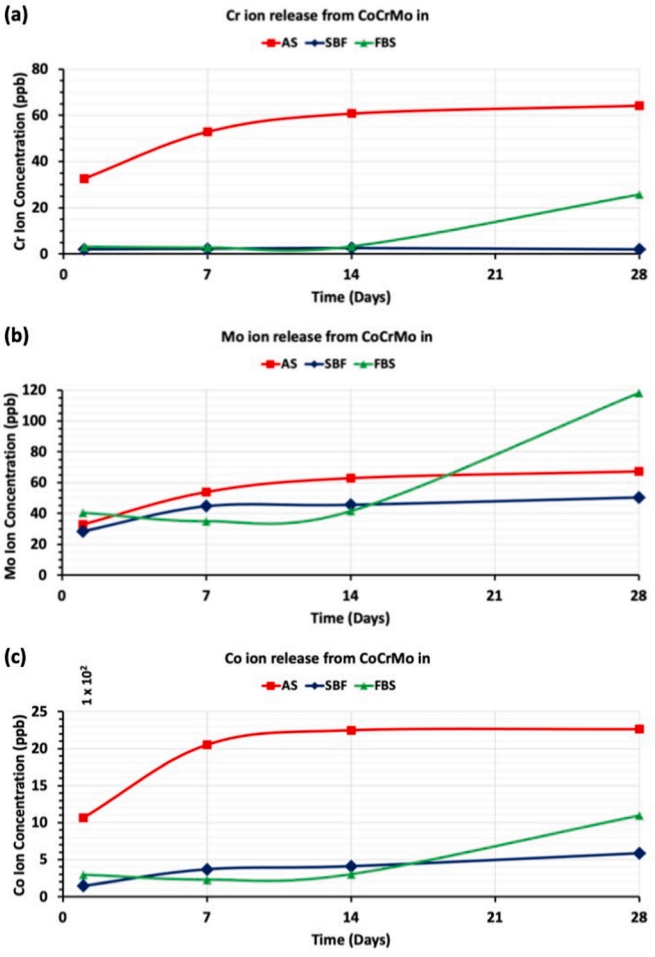

Fig. 2. ICP-MS results showing the **(a)** Cr, **(b)** Mo and **(c)** Co ion release into AS, SBF and FBS upon static immersion for 1, 7, 14 and 28 days.

The source of the highest quantity of ion release into all three immersion fluids was Co (Fig. 2(c)), which can be attributed to the higher solubility of a Co-based oxide layer and the selective dissolution of Co [24]. Indeed, the CoCrMo alloy exhibits a complex ionization behavior independent of the elemental composition. While Cr has the second highest quantity in the current CoCrMo alloy with 27 wt% content, Cr with a 77 wt% presence in the alloy dissolved the least in AS, SBF and FBS following 28 days of static immersion. This aligns well with the previous reports of preferential Co release from CoCrMo and this alloy's complex ion release mechanism [14,27,42].

To further shed light onto the suspected passive oxide layer formation on the CoCrMo alloy in all three immersion fluids and on the chemical reactions between the passive oxide layer and proteins present in FBS, first the surface morphologies of an as-cast CoCrMo sample alongside with the samples immersed the corrosive media for the 28 days were analyzed by SEM (Fig. 3). At a first glance, it is hard to identify any major differences between the surface morphologies of the reference sample (Fig. 3(a)) and the other samples (Fig. 3(b)–(d)). Specifically, polishing marks from surface preparation are visible in all images, yet any severe corrosion-induced depositions or damage to the surface are absent in all images. Indeed, as evident from the SEM images presented in Fig. 3, there is no indication of pitting corrosion in any of the immersed samples; however, the surface of the sample immersed in FBS (Fig. 3(d)) exhibited more deterioration as compared to those of the samples immersed in AS (Fig. 3(b)) and SBF (Fig. 3(c)), indicating enhanced corrosion in the presence of proteins. Nevertheless, the mostly intact appearance of all the immersed samples stands in contrast with the fact that a significant number of ions were released during the immersion experiments. This discrepancy can be explained by the possibility of oxide layer reformation on the surface of the samples during the immersion, obscuring features of the corrosion [18]. Furthermore, a closer look at the surfaces of the samples immersed in SBF showed that there is notable particle precipitation on the surface (Fig. 4).

These observations warranted a thorough inspection of the surface layer, and to begin with, the particles that precipitated on the surfaces of the samples immersed in SBF were analyzed by EDX (Fig. 5), which revealed that these particles contain Ca and O. Although quantitative evaluation of oxygen content by EDX is difficult, this already hints at bone-like hydroxyapatite formation that can facilitate the osseointegration process by improving the interaction between the bone tissue and an implant material [43–45]. In Addition to the Ca^{2+} ion that can enhance the formation of bone-like hydroxyapatite, other ions such as HPO_4^{2-}, CO_3^{2-} that exist in SBF can enhance apatite deposition, which facilitates the osseointegration process [46]. To verify the existence of these species on the surface and understanding the aforementioned formation/reformation cycles of the passive oxide layers on the sample surfaces, the immersed samples were analyzed by XPS (Fig. 6).

During the XPS analyses, the samples were etched for 60 s to remove surface contaminations, followed by subsequent etching for 1080 s. Fig. 6(a) illustrates the peaks of Cr 2p3/2 that are located at 573.5 eV and 576.2 eV for the CoCrMo sample immersed in AS for 28 days, which correspond to Cr^0 and Cr-oxide (Cr^{2+}), respectively. In Fig. 6(b) the binding energies of 574.2 eV and 576.9 eV represent the metallic Cr and Cr^{3+} on the surface, respectively, for the sample immersed in SBF for 28 days. The results of the XPS analysis of the sample immersed in FBS for 28 days are presented in Fig. 6(c), where the 573.1 eV and 576.2 eV binding energies correspond to metallic Cr and Cr-oxide, respectively, which are in agreement with the previously reported values in the literature [47–52]. Moreover, the Cr-oxide layer disappears after an etching time of 120 s. As the etching time further increases, the metallic Cr appears in deeper layers (Fig. 7). For the samples immersed in SBF, the binding energies of Cr at an etching time of 120 s move to 574.3 and

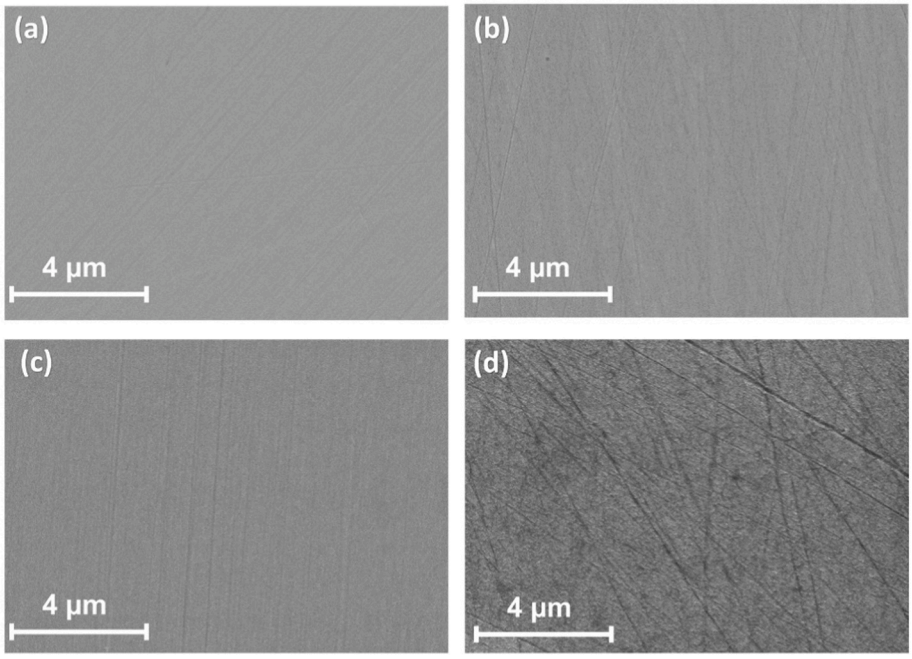

Fig. 3. The SEM micrographs of **(a)** the as-cast CoCrMo sample and the CoCrMo samples immersed in **(b)** AS, **(c)** SBF, and **(d)** FBS for 28 days.

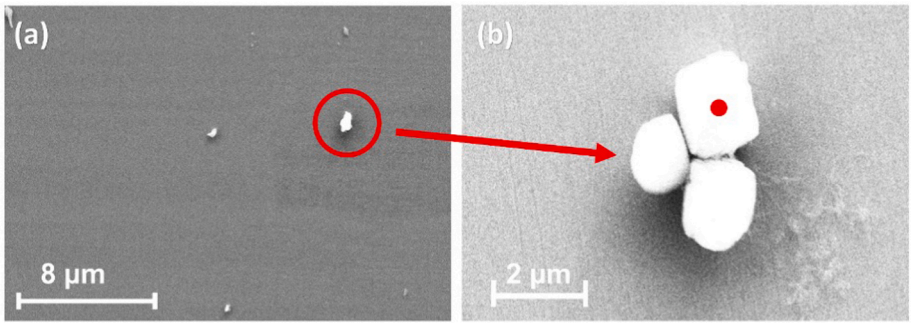

Fig. 4. **(a)** The SEM micrograph of the CoCrMo sample immersed in SBF for 28 days showing precipitation of particles on the surface and **(b)** magnified view of the precipitates. The red dot in (b) indicates the EDX acquisition point (Fig. 5).

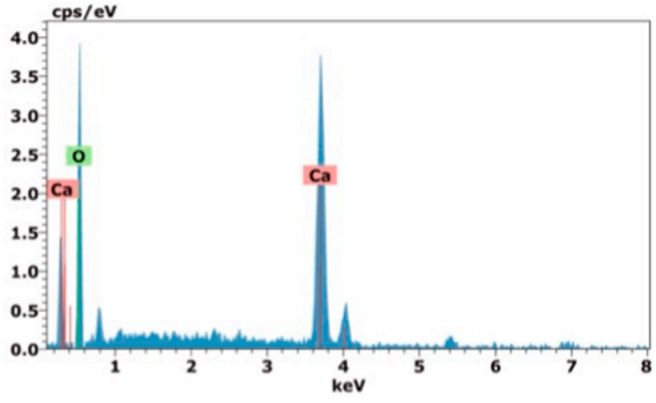

Fig. 5. Representative EDX analysis of precipitated particles observed on the surface of CoCrMo samples (Fig. 4) immersed in SBF for 28 days.

575.6 eV, which evidence the existence of metallic Cr and CrO_3, respectively [53]. This layer diminishes as the etching reveals deeper layers and at an etching time of 480 s the oxide vanishes and metallic Cr with binding energy values of 574.2 and 583.3 eV appears [54]. Additionally, for samples immersed in FBS for 28 days (Fig. 6(c)), the Cr-oxide layer is replaced by metallic Cr with peak values of 573.2 eV and 574.8 eV [54,55] after an etching time of 120 s.

In addition to the Cr oxides on the sample surfaces, Ca and P formations were also observed, highlighting the hydroxyapatite formation (Figs. 7 and 8). Specifically, the peaks of Ca 2p3/2 and 2p1/2 in Fig. 8 support the hydroxyapatite formation on CoCrMo sample surfaces. The samples immersed in AS (Fig. 8(a)) show the binding energy values of 346.9 and 350.4 eV corresponding to the Ca^{2+} ions and CaCO3 formation on the surface of the samples [56–58]; however, this layer is very thin and disappears at an etching time of 120s. The P2p3/2 peak is located at 132.5 eV binding energy (Fig. 9 (a)) indicates phosphate within calcium formation which is the characteristics of the hydroxyapatite formation on the surface [59,60]. For the samples immersed in SBF (Fig. 8(b)), the Ca2p peak occurs at a binding energy of 347.8 eV and its doublet occurs at the 351.2 eV, which is attributed to the Ca^{2+} ions [61,62]. This supports the results of the EDX analysis (Fig. 5) and demonstrates the potential of bone-like hydroxyapatite formation on the sample's surface. In addition, the P peaks with 133.3 eV binding energy were detected on the surface of the sample immersed in SBF (Fig. 9(b)) [59,63–65], showing the formation of natural calcium phosphate on the surface, a compound with the ability to enhance osseointegration

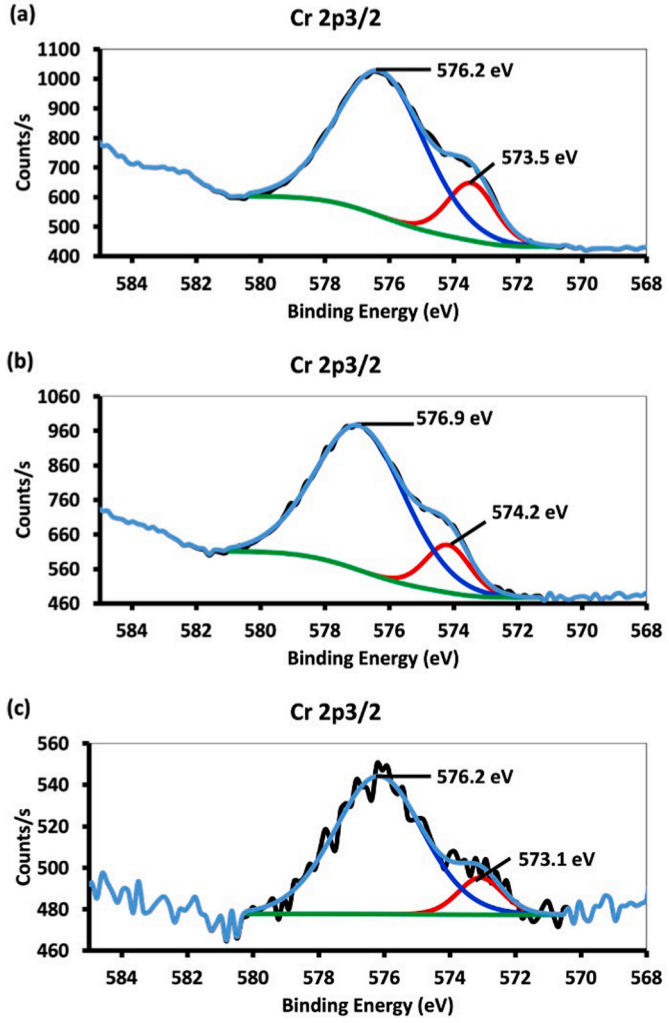

Fig. 6. XPS results prior to etching showing the Cr 2p3/2 snap of CoCrMo samples immersed in **(a)** AS, **(b)** SBF, and **(c)** FBS for 28 days.

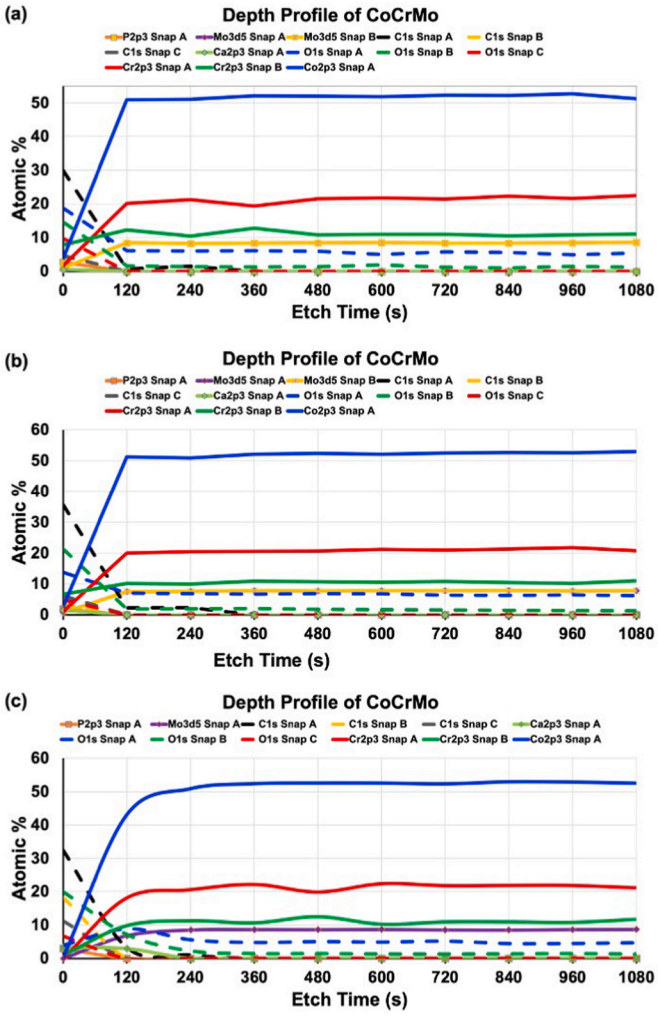

Fig. 7. XPS depth profile of CoCrMo samples immersed in **(a)** AS, **(b)** SBF, and **(c)** FBS for 28 days.

process [63,64]. For the samples immersed in FBS (Fig. 8(c)), the Ca2p3/2 peak at a binding energy of 346.7 and the Ca2p1/2 peak at 350.2 eV binding energy are attributed to Ca^{2+} ions, which facilitate calcite formation, and thus, enhancing the chance of bone-like apatite formation on the surface [62,66]. The corresponding P peaks are presented in Fig. 9(c), where the P2p3/2 peak centered at 132.5 binding energy is associated with calcium phosphate formation [59,60]. However, this layer diminishes as the etching time reaches 120s (Fig. 7).

Overall, the thorough surface analysis presented herein proved that both passive oxide layer and hydroxyapatite formation occur on the CoCrMo sample surfaces immersed in AS, SBF and FBS for 28 days. While the highest rate of Ca and P formation on CoCrMo surface is prevalent in the FBS solution, the least amount of Ca and P formation is observed when the samples are immersed in SBF (Fig. 7). On the other hand, Cr-like passivity is supported more by SBF and AS solutions than by the FBS.

3.2. Cell culture experiments

In an effort to assess the biocompatibility of the CoCrMo alloy from different perspectives, in addition to the static biocompatibility experiments and the corresponding post-mortem chemical characterization, cell culture experiments were also carried out in the current study. Results of the MTT cytotoxicity tests, with the percent (%) viability of Saos-2 cells on the CoCrMo surfaces at incubation periods of 3, 5 and 10 days in comparison with the control group are given in Fig. 10. Accordingly, the cell viability on the CoCrMo surface initially decreases from day 3 to day 5, which is followed by an increase through the 10th day of incubation. Previous research has shown that Mo improves the corrosion resistance of biomedical alloys by providing both a protective layer and preventing pitting corrosion [67]. Therefore, the high cell viability rates on the alloy surfaces can be attributed to the biocompatible character of the CoCrMo alloy, which has also been clearly demonstrated with the aid of static biocompatibility experiments and the corresponding post-mortem chemical characterization results presented herein. The relatively low cell viability on the 5th day of incubation on the other hand, indicates a partial dissolution of the protective oxide layer or formation of cracks within the oxide layer, both of which can result in ion release into the cell culture media. However, the significant increase in cell viability rates on the 10th day of incubation suggests the reformation of a stable oxide layer as incubation proceeded.

The field emission SEM (FESEM) images displaying the cell attachment behavior on the alloy surfaces (Fig. 11) also evidence that the CoCrMo surface provides a favorable environment for cell attachment. Shorter cellular extensions are observed at the early stage of incubation (Fig. 11(a)), which seem to be elongated as incubation proceeds (Fig. 11 (b)). On the 10th day of incubation, cellular networks become evident (Fig. 11(c)). Overall, the evidence of Saos-2 cell viability and proliferation indicates the potential of the CoCrMo alloy to be utilized as an orthopedic implant material.

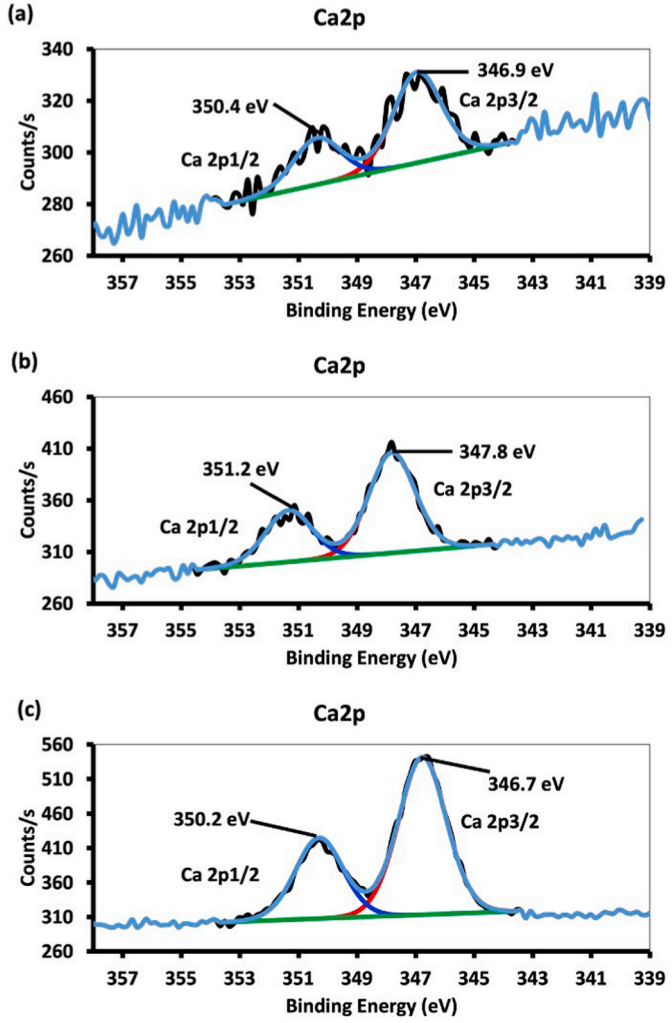

Fig. 8. XPS results prior to etching showing the Ca 2p3/2 and Ca 2p1/2 snaps of CoCrMo samples immersed in **(a)** AS, **(b)** SBF, and **(c)** FBS for 28 days.

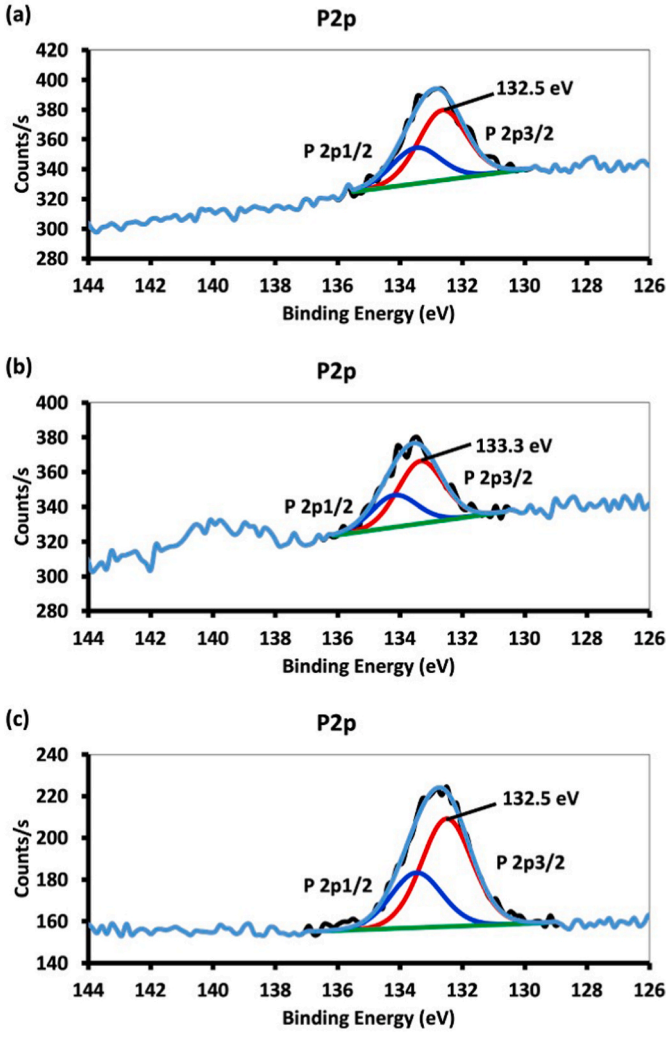

Fig. 9. XPS results prior to etching showing the P 2p3/2 and P 2p1/2 snaps of CoCrMo samples immersed in **(a)** AS, **(b)** SBF, and **(c)** FBS for 28 days.

3.3. Response to medical grade radiation

An important concern when it comes to the presence of permanent implants in human body is how they affect the surrounding tissue during the lifespan of a patient. Even though biocompatibility experiments (both in vivo and in vitro) give researchers a good idea about the expected side effects and benefits, there are certain non-standard situations, such as cancer treatment, that might need to be taken into account for some patients. Considering the ever-increasing rates of cancer diagnosis of all forms, as well as exploring another dimension of biocompatibility analysis, we also investigated the possible effects of a previously implanted CoCrMo medical implant on the radiation dose distribution around the tissue circumventing the implant. In order to simulate a situation where a tumor needs to be treated by radiation therapy in the vicinity of a previously implanted CoCrMo alloy medical implant, CoCrMo samples with dimensions of 10 mm × 5 mm x 1 mm were placed on solid water phantoms (Fig. 12(a)). Normally, for calibration and measurement purposes in linear accelerators used in radiotherapy, water is employed as the reference material. However, owing to the complexity of the mechanical and electronic systems, and the difficulty of installation, usually solid water phantoms are utilized in experiments to simulate live tissue since their density and the number of electrons per gram are equivalent to those of live tissue. In the current study, IBA RW3 solid water phantoms with a density of 1.045 g/cm^3 and an electron density of 3.43 × 10^{23} electron/cm^3 were utilized, and some

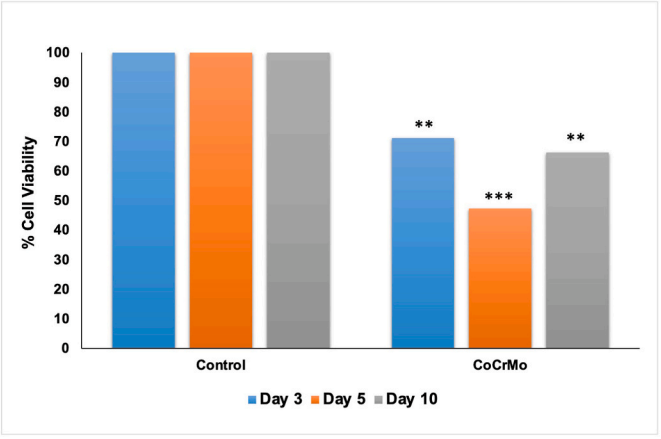

Fig. 10. Cell viability results following 3, 5 and 10 days of incubation of Saos-2 cells on the surface of as-cast CoCrMo samples; while evaluating cell viability, Saos-2 cells incubated in a culture flask were used as the control group (n = 3, ** $p < 0.01$, *** $p < 0.001$); the standard deviation was smaller than 1%, and thus, the error bars are not shown for the sake of clarity of the figure.

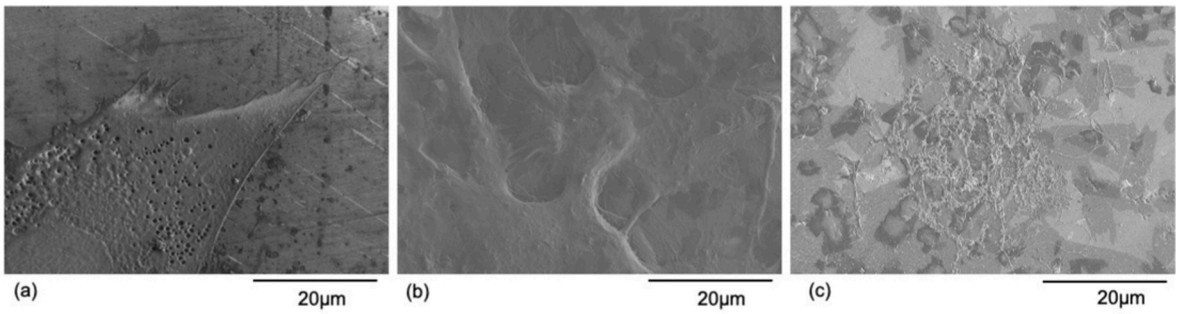

Fig. 11. FESEM images of the Saos-2 cells fixated on CoCrMo surface following **(a)** 3, **(b)** 5, and **(c)** 10 days of incubation.

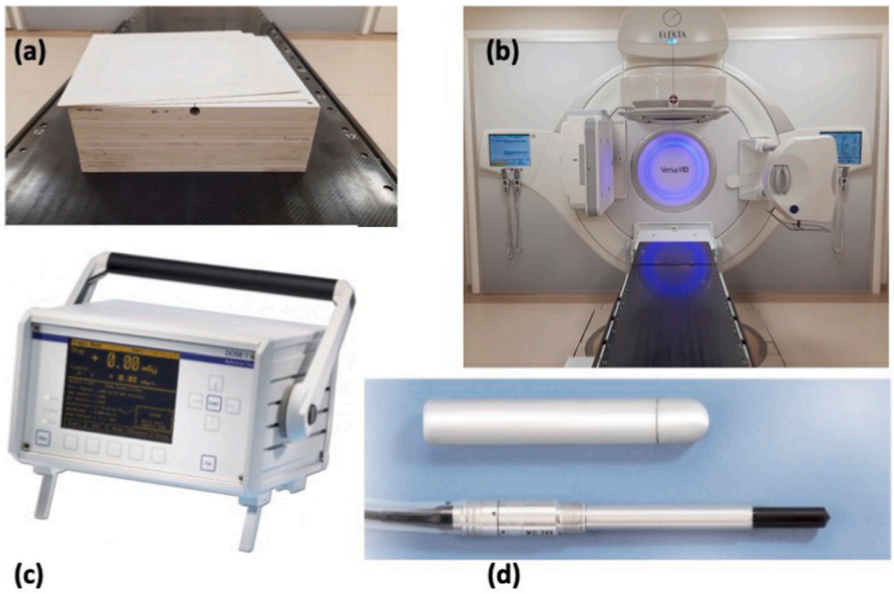

Fig. 12. **(a)** The IBA RW3 solid water phantoms, **(b)** the Elekta Versa HD linear accelerator, **(c)** the IBA Dose 1 electrometer, and **(d)** the IBA FC65 Farmer type ion capsules employed in the current irradiation study.

of the phantoms had an opening for placing the ion capsules. The phantoms utilized in the current experiments had dimensions of 30 cm × 30 cm x 1 cm.

The linear accelerator employed in this work was an Elekta Versa HD (Fig. 12(b)) featuring 6 MV, 10 MV, 15 MV, 6 MV FFF and 10 MV FFF photon energy levels, and 6 MeV, 9 MeV, 12 MeV and 15 MeV electron energy levels. The accelerator also features a multi leaf collimator (MLC) system with 80 pairs of leaves with a width of 0.5 cm at source to surface distance (SSD) of 100 cm. The accelerator houses an X-ray volume imaging (XVI) system to monitor tumors and critical tissue nearby, and to position the patient prior to treatment. The dose distributions are measured utilizing the iViewGT system and the corresponding data is processed with the Mosaiq software. The measurement of the current that stems from irradiation was measured utilizing an IBA Dose 1 electrometer (Fig. 12(c)) with a 0–500 V polarization voltage and a current measurement range of 40 pA–1000 nA. For electron bundle measurements, an IBA FC65 Farmer type ion capsule (Fig. 12(d)) was employed with a voltage range of 100–400 V.

Once the samples were placed on the water phantoms, CT scans of the samples were taken and fed into a Monaco TPS for irradiation with 100 cGy utilizing a photon beam of 6 MV. Point dose radiation measurements were made for lateral distances up to 2 cm from the center of CoCrMo samples in each direction with an interval of 0.5 cm, and the radiation dose variation from the sample surfaces to 2 cm depth from the samples was monitored with a 0.5 cm interval (Fig. 13). The results demonstrate that the presence of CoCrMo in tissue undergoing radiation

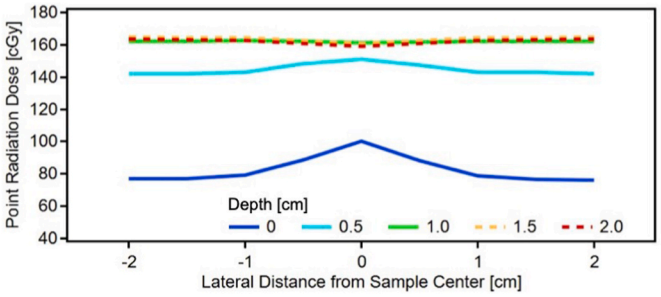

Fig. 13. Variation of the point dose distribution within the solid water phantoms with depth (from surface) and lateral distance from the sample center.

therapy does not significantly change the radiation dose distribution at non-zero depths. In other words, in the case where a CoCrMo implant is in the way of photons targeting a tumor, the effect of the implant on the actual radiation dose induced upon the malignant tissue will be minimal. In addition, the results corresponding to the depths of 0 and 0.5 cm indicate that the radiation accumulation in the tissue within the immediate vicinity of a CoCrMo implant would be a minimum, eliminating some of the undesired side effects.

4. Conclusions

A CoCrMo medium entropy alloy composed of 27 wt% Cr, 6 wt% Mo and balance Co was subjected to static immersion, cell culture and radiation experiments in order to evaluate its potential to be utilized as a dental and orthopedic implant material from a broader perspective. The static immersion experiments conducted in artificial saliva (AS), simulated body fluid (SBF) and fetal bovine serum (FBS), and the post-mortem chemical analyses have demonstrated that both passive oxide layer and hydroxyapatite formation were evident on the CoCrMo sample surfaces upon immersion in all three biological media for 28 days. Specifically, the highest rate of Ca and P formation on CoCrMo surface was prevalent in the FBS solution, while the least amount of Ca and P formation was observed upon immersion in SBF. In addition, Cr-like passivity was more prevalent in SBF and AS than in the FBS. These findings were also supported by the cell culture experiments, such that the evidence of Saos-2 cell viability and proliferation indicated the potential of the CoCrMo alloy to be utilized as an orthopedic implant material. Finally, the scenario of a CoCrMo implant standing in the way of photon beams during a radiation therapy was also considered by applying medical grade radiation to water phantoms circumventing CoCrMo samples. The results of the experiments carried out in an accelerator showed that the radiation accumulation in the tissue within the immediate vicinity of a CoCrMo implant remained a minimum, eliminating some of the undesired side effects. Overall, the experimental findings presented herein clearly demonstrate the high potential of the CoCrMo medium entropy alloy investigated in this study to be utilized as a safe implant material in dental and orthopedic implants.

Author statement

Seyma Gurel: Formal analysis, Investigation, Writing – Original Draft; Alireza Nazarahari: Formal analysis, Investigation, Writing – Original Draft; Demircan Canadinc: Conceptualization, Resources, Writing – Original Draft, Supervision, Project administration, Funding acquisition; Gregory Gerstein: Formal analysis, Investigation, Writing – Original Draft; Hans J. Maier: Resources, Writing – Original Draft, Supervision, Project administration, Funding acquisition; Haluk Cabuk: Writing – Original Draft, Supervision, Project administration, Taylan Bukulmez: Resources, Formal analysis, Investigation, Writing – Original Draft; Mert Cananoglu: Resources, Formal analysis, Investigation, Writing – Original Draft; M.B. Yagci: Formal analysis, Investigation, Writing – Original Draft; S. Mine Toker: Resources, Writing – Original Draft, Supervision, Project administration, Funding acquisition; Sibel Gunes: Resources, Formal analysis, Investigation, Writing – Original Draft; Merve N. Soykan: Resources, Formal analysis, Investigation, Writing – Original Draft.

Declaration of competing interest

The authors declare that they have no known competing financial interests or personal relationships that could have appeared to influence the work reported in this paper.

Data availability

Data will be made available on request.

Acknowledgments

This study was supported by the BAGEP Award of the Science Academy. The authors also acknowledge the financial support by the Koç University Graduate School of Sciences and Engineering. The German part of the study was supported by Deutsche Forschungsgemeinschaft (project number 426335750). S.M. Toker acknowledges the support by Eskisehir Osmangazi University BAP research funds (Grant 2018/15038).

References

[1] A. Marti, Cobalt-base alloys used in bone surgery, Injury 31 (2000) 18–21.
[2] M.K. Amstutz Hc, P. Campbell, H. McKellop, T.P. Schmalzreid, W.J. Gillespie, D. Howie, J. Jacobs, J. Medley, Metal on metal total hip replacement workshop consensus document, Clin. Orthop. Relat. Res. 329 (1996) 297–303.
[3] A.H. Doorn Pf, J.M. Mirra, P.A. Campbell, Tissue reaction to metal on metal total hip prostheses, Clin. Orthop. Relat. Res. 329 (1996) 187–205.
[4] U.R. Jacobs Jj, J.L. Gilbert, Corrosion of metal orthopaedic implants, Am. J. Bone Jt. Surg. 80A (1998) 268–282.
[5] J.J. Hallab N, K. Merritt, Metal sensitivity in patients with orthopaedic implants, Am. J. Bone Jt. Surg. 83A (2001) 428–436.
[6] L.C. Willert Hg, G.H. Buchhorn, A. Fayyazi, R. Flury, M. Windler, G. Köster, Metal-on-metal bearings and hypersensitivity in patients with artificial hip joints, J. Bone Jt. Surg. Am. 87 (2005) 28–36.
[7] C.M. Valko M, H. Morris, Metals, toxicity and oxidative stress, Curr. Med. Chem. 12 (2005) 1161–1208.
[8] F.W. Sunderman Jr., Carcinogenicity of metal alloys in orthopedic prostheses: clinical and experimental studies, Fund. Appl. Toxicol. 13 (1989) 205–216.
[9] W.C. Nouri A, P.D. Hodgson, Biomimetic porous titanium scaffolds for orthopaedic and dental applications, in: Biomimetics, Learn, from Nat., 2009, pp. 415–450.
[10] M.M. Dewidar, H.C. Yoon, J.K. Lim, Mechanical properties of metals for biomedical applications using powder metallurgy process: a review, Met. Mater. Int. 12 (2006) 193–206, https://doi.org/10.1007/BF03027531.
[11] N. Espallargas, C. Torres, A.I. Muñoz, A metal ion release study of CoCrMo exposed to corrosion and tribocorrosion conditions in simulated body fluids, Wear 332–333 (2015) 669–678, https://doi.org/10.1016/j.wear.2014.12.030.
[12] K. Hazlehurst, C.J. Wang, M. Stanford, Evaluation of the stiffness characteristics of square pore CoCrMo cellular structures manufactured using laser melting technology for potential orthopaedic applications, Mater. Des. 51 (2013) 949–955, https://doi.org/10.1016/j.matdes.2013.05.009.
[13] D.A. Puleo, W.W. Huh, Acute toxicity of metal ions in cultures of osteogenic cells derived from bone marrow stromal cells, J. Appl. Biomater. 6 (1995) 109–116, https://doi.org/10.1002/jab.770060205.
[14] A.W.E. Hodgson, S. Kurz, S. Virtanen, V. Fervel, C.O.A. Olsson, S. Mischler, Passive and transpassive behaviour of CoCrMo in simulated biological solutions, Electrochim. Acta 49 (2004) 2167–2178, https://doi.org/10.1016/j.electacta.2003.12.043.
[15] F. Contu, B. Elsener, H. Böhni, Corrosion behaviour of CoCrMo implant alloy during fretting in bovine serum, Corrosion Sci. 47 (2005) 1863–1875, https://doi.org/10.1016/j.corsci.2004.09.003.
[16] I. Milošev, H.H. Strehblow, The composition of the surface passive film formed on CoCrMo alloy in simulated physiological solution, Electrochim. Acta 48 (2003) 2767–2774, https://doi.org/10.1016/S0013-4686(03)00396-7.
[17] I. Milošev, M. Metikoš-Huković, H.H. Strehblow, Passive film on orthopaedic TiAlV alloy formed in physiological solution investigated by X-ray photoelectron spectroscopy, Biomaterials 21 (2000) 2103–2113, https://doi.org/10.1016/S0142-9612(00)00145-9.
[18] S.M. Toker, D. Canadinc, H.J. Maier, O. Birer, Evaluation of passive oxide layer formation-biocompatibility relationship in NiTi shape memory alloys: geometry and body location dependency, Mater. Sci. Eng. C 36 (2014) 118–129, https://doi.org/10.1016/j.msec.2013.11.040.
[19] I.D. Dimić, I.L. Cvijović-Alagić, I.T. Kostić, A.A. Perić-Grujić, M.P. Rakin, S.S. Putić, B.M. Bugarski, OtpuŠtanje metalnih jona iz biokompatibilne legure kobalta, Chem. Ind. Chem. Eng. Q. 20 (2014) 571–577, https://doi.org/10.2298/CICEQ130813039D.
[20] C. Seethalakshmi, R.C. Jagat Reddy, N. Asifa, S. Prabhu, Correlation of salivary pH, incidence of dental caries and periodontal status in diabetes mellitus patients: a cross-sectional study, J. Clin. Diagn. Res. 10 (2016), https://doi.org/10.7860/JCDR/2016/16310.7351. ZC12–ZC14.
[21] J. Qiu, W.Q. Yu, F.Q. Ohang, R.J. Smales, Y.L. Ohang, C.H. Lu, Corrosion behaviour and surface analysis of a Co-Cr and two Ni-Cr dental alloys before and after simulated porcelain firing, Eur. J. Oral Sci. 119 (2011) 93–101, https://doi.org/10.1111/j.1600-0722.2011.00791.x.
[22] C. Valero Vidal, A. Igual Muñoz, Effect of physico-chemical properties of simulated body fluids on the electrochemical behaviour of CoCrMo alloy, Electrochim. Acta 56 (2011) 8239–8248, https://doi.org/10.1016/j.electacta.2011.06.068.
[23] I. Mutlu, E. Oktay, Characterization of 17-4 PH stainless steel foam for biomedical applications in simulated body fluid and artificial saliva environments, Mater. Sci. Eng. C 33 (2013) 1125–1131, https://doi.org/10.1016/j.msec.2012.12.004.
[24] M. Metikoš-Huković, Z. Pilić, R. Babić, D. Omanović, Influence of alloying elements on the corrosion stability of CoCrMo implant alloy in Hank's solution, Acta Biomater. 2 (2006) 693–700, https://doi.org/10.1016/j.actbio.2006.06.002.
[25] Z. Guo, X. Pang, Y. Yan, K. Gao, A.A. Volinsky, T.Y. Zhang, CoCrMo alloy for orthopedic implant application enhanced corrosion and tribocorrosion properties by nitrogen ion implantation, Appl. Surf. Sci. 347 (2015) 23–34, https://doi.org/10.1016/j.apsusc.2015.04.054.
[26] X. Yang, N. Xiang, B. Wei, Effect of fluoride content on ion release from cast and selective laser melting-processed Co-Cr-Mo alloys, J. Prosthet. Dent 112 (2014) 1212–1216, https://doi.org/10.1016/j.prosdent.2013.12.022.
[27] D. Ionita, C. Ungureanu, I. Demetrescu, Electrochemical and antibacterial performance of CoCrMo alloy coated with hydroxyapatite or silver nanoparticles,

J. Mater. Eng. Perform. 22 (2013) 3584–3591, https://doi.org/10.1007/s11665-013-0653-5.
[28] N. Rinčić, I. Baučić, S. Miko, M. Papić, E. Prohić, Corrosion behaviour of the Co-Cr-Mo dental alloy in solutions of different composition and different pH values, Coll. Antropol. 27 (2003) 99–106.
[29] M. Hurlbutt, B. Novy, D. Young, Dental caries: a pH-mediated disease, J. Calif Dent. Hyg. Assoc. 25 (2010) 9–15.
[30] S.M. Toker, D. Canadinc, Evaluation of the biocompatibility of NiTi dental wires : a comparison of laboratory experiments and clinical conditions, Mater. Sci. Eng. C 40 (2014) 142–147, https://doi.org/10.1016/j.msec.2014.03.060.
[31] L. Freire, M.A. Catarino, M.I. Godinho, M.J. Ferreira, M.G.S. Ferreira, A.M. P. Simões, M.F. Montemor, Electrochemical and analytical investigation of passive films formed on stainless steels in alkaline media, Cem. Concr. Compos. 34 (2012) 1075–1081, https://doi.org/10.1016/j.cemconcomp.2012.06.002.
[32] W. Rostoker, J.O. Galante, P. Lereim, Evaluation of couple/crevice corrosion by prosthetic alloys under in vivo conditions, J. Biomed. Mater. Res. 12 (1978) 823–829, https://doi.org/10.1002/jbm.820120605.
[33] E.K. Ocran, L.E. Guenther, J.M. Brandt, U. Wyss, O.A. Ojo, Corrosion and fretting corrosion studies of medical grade CoCrMo alloy in a clinically relevant simulated body fluid environment, Metall. Mater. Trans. A Phys. Metall. Mater. Sci. 46 (2015) 2696–2709, https://doi.org/10.1007/s11661-015-2834-3.
[34] K.V. Honn, J.A. Singley, W. Chavin, Fetal bovine serum: a multivariate standard, Proc. Soc. Exp. Biol. Med. 149 (1975) 344–347, https://doi.org/10.3181/00379727-149-38804.
[35] G. Gstraunthaler, T. Lindl, J. Van Der Valk, A plea to reduce or replace fetal bovine serum in cell culture media, Cytotechnology 65 (2013) 791–793, https://doi.org/10.1007/s10616-013-9633-8.
[36] M.G. McAlinden, D.J. Wilson, Comparison of cancellous bone-derived cell proliferation in autologous human and fetal bovine serum, Cell Transplant. 9 (2000) 445–451, https://doi.org/10.1177/096368970000900401.
[37] R. Hang, S. Ma, V. Ji, P.K. Chu, Corrosion behavior of NiTi alloy in fetal bovine serum, Electrochim. Acta 55 (2010) 5551–5560, https://doi.org/10.1016/j.electacta.2010.04.061.
[38] F. Contu, B. Elsener, H. Böhni, Characterization of implant materials in fetal bovine serum and sodium sulfate by electrochemical impedance spectroscopy. II. Coarsely sandblasted samples, J. Biomed. Mater. Res., Part A 67 (2003) 246–254, https://doi.org/10.1002/jbm.a.10113.
[39] T. Kokubo, H. Takadama, How useful is SBF in predicting in vivo bone bioactivity? Biomaterials 27 (2006) 2907–2915, https://doi.org/10.1016/j.biomaterials.2006.01.017.
[40] K. Yamanaka, M. Mori, A. Chiba, Enhanced mechanical properties of As-forged Co-Cr-Mo-N alloys with ultrafine-grained structures, Metall. Mater. Trans. A Phys. Metall. Mater. Sci. 43 (2012) 5243–5257, https://doi.org/10.1007/s11661-012-1288-0.
[41] B. Uzer, O. Birer, D. Canadinc, Investigation of the dissolution–reformation cycle of the passive oxide layer on NiTi orthodontic archwires, Shape Mem. Superelasticity. 3 (2017) 264–273, https://doi.org/10.1007/s40830-017-0114-3.
[42] T. Hanawa, Metal ion release from metal implants, Mater. Sci. Eng. C 24 (2004) 745–752, https://doi.org/10.1016/j.msec.2004.08.018.
[43] T. Miyazaki, H.-M. Kim, T. Kokubo, C. Ohtsuki, H. Kato, T. Nakamura, Mechanism of bonelike apatite formation on bioactive tantalum metal in a simulated body fluid, Biomaterials 23 (2002) 827–832, https://doi.org/10.1016/S0142-9612(01)00188-0.
[44] J.W. Park, K.B. Park, J.Y. Suh, Effects of calcium ion incorporation on bone healing of Ti6Al4V alloy implants in rabbit tibiae, Biomaterials 28 (2007) 3306–3313, https://doi.org/10.1016/j.biomaterials.2007.04.007.
[45] R. Godley, D. Starosvetsky, I. Gotman, Bonelike apatite formation on niobium metal treated in aqueous NaOH, J. Mater. Sci. Mater. Med. 15 (2004) 1073–1077, https://doi.org/10.1023/B:JMSM.0000046388.07961.81.
[46] X. Zhang, Z.M. Xiu, X.W. Li, Preparation and characterization of (HAp/SiO_2)/Ti biocomposites, Adv. Mater. Res. 217–218 (2011) 88–92. https://doi.org/10.4028/www.scientific.net/AMR.217-218.88.
[47] H.R. Nawaz, B.A. Solangi, K. Pervez, F. Ahmed, H. Cao, Synthesis and characterization of partially metallic chromium hollow nanospheres: a step toward the tuning of magnetic property, J. Chem. Soc. Pakistan 39 (2017) 391–398.
[48] A. Conde, A.B. Cristóbal, G. Fuentes, T. Tate, J. de Damborenea, Surface analysis of electrochemically stripped CrN coatings, Surf. Coating. Technol. 201 (2006) 3588–3595, https://doi.org/10.1016/j.surfcoat.2006.08.110.
[49] B. Choudhary, D. Paul, A. Singh, T. Gupta, Removal of hexavalent chromium upon interaction with biochar under acidic conditions: mechanistic insights and application, Environ. Sci. Pollut. Res. 24 (2017) 16786–16797, https://doi.org/10.1007/s11356-017-9322-9.
[50] Y. Chen, K. Ding, L. Yang, B. Xie, F. Song, J. Wan, G. Wang, M. Han, Nanoscale ferromagnetic chromium oxide film from gas-phase nanocluster deposition, Appl. Phys. Lett. 92 (2008) 29–32, https://doi.org/10.1063/1.2919077.
[51] R. Cheng, B. Xu, C.N. Borca, A. Sokolov, C.S. Yang, L. Yuan, S.H. Liou, B. Doudin, P. A. Dowben, Characterization of the native Cr2O3 oxide surface of CrO2, Appl. Phys. Lett. 79 (2001) 3122–3124, https://doi.org/10.1063/1.1416474.
[52] R. Cheng, C.N. Borca, N. Pilet, B. Xu, L. Yuan, B. Doudin, S.H. Liou, P.A. Dowben, Oxidation of metals at the chromium oxide interface, Appl. Phys. Lett. 81 (2002) 2109–2111, https://doi.org/10.1063/1.1506942.
[53] M.C. Biesinger, B.P. Payne, A.P. Grosvenor, L.W.M. Lau, A.R. Gerson, R.S.C. Smart, Resolving surface chemical states in XPS analysis of first row transition metals, oxides and hydroxides: Cr, Mn, Fe, Co and Ni, Appl. Surf. Sci. 257 (2011) 2717–2730, https://doi.org/10.1016/j.apsusc.2010.10.051.
[54] G.C. Allen, P.M. Tucker, R.K. Wild, X-ray photoelectron/Auger electron spectroscopic study of the initial oxidation of chromium metal, J. Chem. Soc. Faraday Trans. 2 Mol. Chem. Phys. 74 (1978) 1126–1140, https://doi.org/10.1039/F29787401126.
[55] T.A. Dang, C.N. Chau, Electron spectroscopy for chemical analysis of cool white phosphors coated with SiO2 thin film, J. Electrochem. Soc. 143 (1996) 302–305, https://doi.org/10.1149/1.1836427.
[56] T.A. Patterson, J.C. Carver, D.E. Leyden, D.M. Hercules, A surface study of cobalt-molybdena-alumina catalysts using X-ray photoelectron spectroscopy, J. Phys. Chem. 80 (1976) 1700–1708, https://doi.org/10.1021/j100556a011.
[57] M. Adil, P.K. Dutta, S. Mitra, An aqueous Ca-ion full cell comprising BaHCF cathode and MCMB anode, ChemistrySelect 3 (2018) 3687–3690, https://doi.org/10.1002/slct.201800419.
[58] H. Sebei, D. Pham Minh, A. Nzihou, P. Sharrock, Sorption behavior of Zn(II) ions on synthetic apatitic calcium phosphates, Appl. Surf. Sci. 357 (2015) 1958–1966, https://doi.org/10.1016/j.apsusc.2015.09.158.
[59] H.Y. Shin, J.Y. Jung, S.W. Kim, W.K. Lee, XPS analysis on chemical properties of calcium phosphate thin films and osteoblastic HOS cell responses, J. Ind. Eng. Chem. 12 (2006) 476–483.
[60] S.J. Park, B.S. Kim, K.C. Gupta, D.Y. Lee, I.K. Kang, Hydroxyapatite nanorod-modified sand blasted titanium disk for endosseous dental implant applications, Tissue Eng. Regen. Med. 15 (2018) 601–614, https://doi.org/10.1007/s13770-018-0151-9.
[61] B. Demri, D. Muster, XPS study of some calcium compounds, J. Mater. Process. Technol. 55 (1995) 311–314, https://doi.org/10.1016/0924-0136(95)02023-3.
[62] J. Baltrusaitis, C.R. Usher, V.H. Grassian, Reactions of sulfur dioxide on calcium carbonate single crystal and particle surfaces at the adsorbed water carbonate interface, Phys. Chem. Chem. Phys. 9 (2007) 3011–3024, https://doi.org/10.1039/b617697f.
[63] T. Hanawa, S. Hiromoto, A. Yamamoto, D. Kuroda, K. Asami, XPS characterization of the surface oxide film of 316L stainless steel samples that were located in quasi-biological environments, Mater. Trans. 43 (2002) 3088–3092, https://doi.org/10.2320/matertrans.43.3088.
[64] T. Hanawa, M. Ota, Calcium phosphate naturally formed on titanium in electrolyte solution, Biomaterials 12 (1991) 767–774, https://doi.org/10.1016/0142-9612(91)90028-9.
[65] T. Hanawa, M. Ota, Characterization of surface film formed on titanium in electrolyte using XPS, Appl. Surf. Sci. 55 (1992) 269–276, https://doi.org/10.1016/0169-4332(92)90178-Z.
[66] M. Ni, B.D. Ratner, Differentiating calcium carbonate polymorphs by surface analysis techniques - an XPS and TOF-SIMS study, Surf. Interface Anal. 40 (2008) 1356–1361, https://doi.org/10.1002/sia.2904.
[67] A.A. Rodriguez, J.H. Tylczak, M.C. Gao, P.D. Jablonski, M. Detrois, M. Ziomek-Moroz, J.A. Hawk, Effect of molybdenum on the corrosion behavior of high-entropy alloys CoCrFeNi 2 and CoCrFeNi 2 Mo 0.25 under sodium chloride aqueous conditions, Adv. Mater. Sci. Eng. 2018 (2018) 1–11, https://doi.org/10.1155/2018/3016304.